# Copper zinc aluminate synthesized by sol-gel method with polyacrylic acid as catalysts for glycerol hydrogenolysis

Dr. Lama Omar,[1] Dr. Thomas Onfroy,[2] Prof. Stéphane Daniele,[1] Dr. Noémie Perret[1,*]

[1] *Univ Lyon, Université Claude Bernard Lyon 1, CNRS, IRCELYON, F-*69626, Villeurbanne, France.

[2] *Sorbonne Université, CNRS, Laboratoire de Réactivité de Surface, F-75005 Paris, France*

*corresponding author: noemie.perret@ircelyon.univ-lyon1.fr

## Abstract

This study describes the use of novel Cu/ZnO/$ZnAl_2O_4$/PAAH (PAAH = polyacrylic acid) hybrid nanomaterials for glycerol hydrogenolysis. Their elaboration by sol-gel process either in one step or in two steps allowed to modulate their structural properties in terms of specific surface area, Lewis acidity, sizes and dispersion of copper nanoparticles. The presence of PAAH and aluminium during the synthesis particularly showed benefits in terms of dispersion and metal-support interaction. The characterization of the catalyst surfaces in composition and size of the copper nanoparticles allowed to establish structure-reactivity relationships. Their optimization allowed to reach remarkable conversions up to 96% with selectivity towards 1,2-propanediol of 83%. A recyclability study also showed a possible reuse of these catalysts after a reactivation step.

## Keywords

Glycerol; sol-gel processes; copper; polyacrylic acid; zinc aluminate

## Introduction

The valorization of glycerol, co-produced during the production of biodiesel, is still a major challenge.[1] 1,2-propanediol is an important commodity chemical with a wide range of applications, including antifreeze additive, de-icing fluid, and polyester resins.[1] The synthesis of this later compound from glycerol has been widely studied, but the development of a cost-effective process remains difficult.[2] A number of noble (e.g. Ru, Rh, Pt)[3–5] and non-noble (e.g. Cu, Ni)[6] metal catalysts have been tested for the hydrogenolysis of glycerol. Catalysts based on noble metals usually exhibit high activity but low selectivity towards 1,2-propanediol, due to C-C bond cleavage.[3] A review of the literature indicates that the most promising catalysts are copper-based, and many studies have focused on their design[2,6–8]. Different supports have been employed, including ZnO,[9–13] $Al_2O_3$,[13–16] $CeO_2$,[17] $TiO_2$,[13,14] $SiO_2$[13,18–21] and some aluminosilicates,[15] $ZrO_2$,[13,22–24] and MgO[13,22,25–28]. There is a general consensus that bifunctional catalysts with metallic Cu sites as well as (Brønsted and/or Lewis) acidic sites favor the selective formation of propanediols. Thus, the support

plays a crucial role in the catalytic performance. Different studies have shown that Cu/ZnO catalysts exhibit high selectivity towards 1,2-propanediol in the range of 77% to 100%, however the conversion generally remains below 50%.[9–11,29–32] Additionally, Cu/ZnO catalysts usually undergo strong deactivation when used in water, due to metal leaching, loss of surface area and sintering of ZnO and Cu nanoparticles.[12,32,33] It is worth noting that $Cu/ZnO/Al_2O_3$ may exhibit improved catalytic properties for the conversion of glycerol, especially in terms of stability, due to the presence of aluminum.[34,35]

For the hydrogenolysis of glycerol, Cu-Zn and Cu-Zn-Al systems have principally been synthesized by the traditional impregnation and co-precipitation methods.[9–12,31,34,36–39] Other studies report the use of solid state fusion[40] or evaporation-induced self-assembly[41]. It is known that the synthesis method can affect the physico-chemical properties of catalysts. It was shown that the precipitating agents in co-precipitation and solid-state fusion followed by precipitation methods affected the Cu crystallite size and the strength of (Brønsted and Lewis) acid sites.[40] Of particular relevance to this study is the work of *P*. Claus *et al.* [30] who reported higher glycerol conversion (46% vs. 17%) for Cu/ZnO prepared by an oxalate gel method than the one synthesized by co-precipitation method due to their higher copper surface area (30 vs. 17 $m^2\ g^{-1}_{Cu}$). After incorporation of Al,[42] 76% yield towards 1,2-propanediol was obtained employing $Cu\text{-}ZnO\text{-}Al_2O_3$ with high catalyst (72 $m^2\ g^{-1}_{catalyst}$) and copper (117 $m^2\ g^{-1}_{Cu}$) surface area. We reported in a first study, the synthesis, by sol-gel method, of ZnO support with high surface area (up to 120 $m^2\ g^{-1}$). After addition of Cu nanoparticles, these catalysts showed much higher conversion than when employing commercial ZnO (70% *vs.* 25%). There is only one report in the literature of the hydrogenolysis of glycerol over Cu-Zn-Al systems with high surface area synthesized by sol-gel method (175 $m^2\ g^{-1}$).[35] High yield towards propylene glycol (≈ 90%) was obtained in a continuous-flow reactor for ca. 5 h, then the catalyst strongly deactivated due to coke formation along with Cu sintering. The catalyst was prepared following a multi-steps method with aluminium isopropoxide, copper nitrate, zinc nitrate, ethylene glycol, nitric acid and ammonia.

The preparation of supported metal catalysts by sol-gel processing provides solid with distinct catalytic properties.[43] Sol-gel synthesis generates materials with high surface area and homogeneous distribution of active species. Preparations can be made in one step and additional elements can easily be added. Finally, catalysts made by sol-gel method have been shown to exhibit improved tolerance to thermal treatment[44] and metal sintering[45] for other reactions of interest.

In this work, we developed a one pot sol-gel method with trimethylaluminium, diethylzinc, copper nitrate and polyacrylic acid for the synthesis of Cu-Zn-Al catalysts. We then investigated the catalytic action of these systems in the hydrogenolysis of glycerol directed at the selective formation of 1,2-propanediol. Finally, the impact of sol-gel method on the physico-chemical properties and the active sites of these systems were examined.

## Results and discussion

### Synthesis and characterization of the catalysts

The syntheses of the different catalysts differed only i) in the composition of the medium and ii) the method of synthesis of the Cu/$ZnAl_xO_y$ solid, starting from hydrolysis of zinc and aluminium alkyl metal precursors. In one case, deposition-precipitation of Cu nitrate with urea were conducted after sol-gel synthesis and isolation of the $ZnAl_xO_y$ support (two steps synthesis – S2) and in the other case the synthesis of the support and deposition-precipitation of Cu nitrate were carried out in the same medium (one step synthesis – S1), following Figure 1.

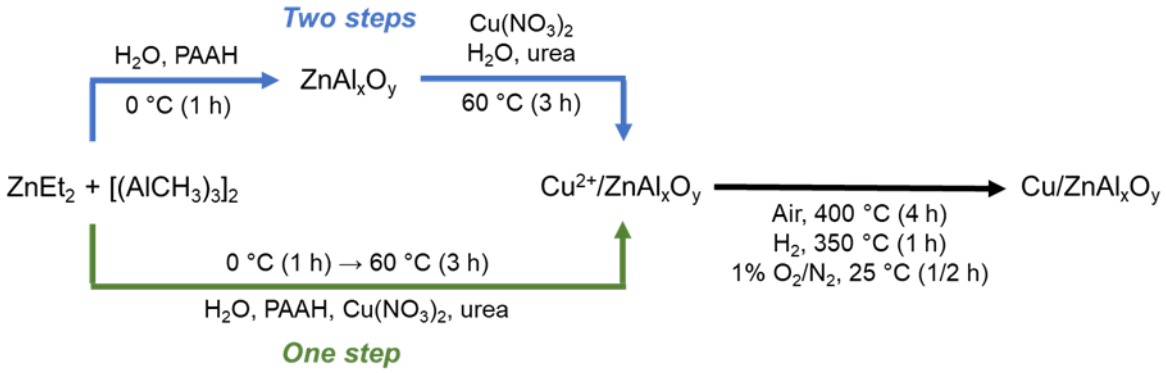


Figure 1. Schematization of the two synthetic routes studied

### Synthesis and characterization of the catalysts synthesized by one step method

The aim of this study was to investigate whether a one-step route (simultaneous presence of PAAH and $Cu^{2+}$ during the elaboration of $ZnAl_xO_y$) could result in materials with stable Al/Zn ratio, high copper dispersion, high specific surface area and efficient catalytic properties. The physico-chemical characteristics of these catalysts will be assessed and correlated to the performances in the hydrogenolysis of glycerol.

**Table 1.** Cu/$ZnAl_xO_y$-S1 and Cu/ZnO-S1 synthesized by one step sol-gel method: main textural and structural properties

| Entry | Catalysts | $n_{Cu}/n_{Zn}$ [a] | $n_{Al}/n_{Zn}$ [a] | $Cu_s$ ($\mu mol_{Cu}\ g^{-1}$) [b] | Surface area ($m^2\ g^{-1}$) [c] | $T_{reduction}$ (°C) [d] |
|---|---|---|---|---|---|---|
| 1 | 4Cu-11Al-S1 | 0.08 | 0.47 | 136 | 143 | 230 |
| 2 | 9Cu-11Al-S1 | 0.18 | 0.49 | 196 | 154 | 246 |
| 3 | 11Cu-11Al-S1 | 0.23 | 0.56 | 216 | 76 | 250 |
| 4 | 18Cu-24Al-S1 | 1.18 | 3.68 | 328 | 265 | 249 |
| 5 | 25Cu-16Al-S1 | 0.89 | 1.39 | 382 | 97 | 246 |
| 6 | 21Cu-S1 | 0.32 | - | 72 | 24 | 219 |
| 7 | 11Cu-11Al-S1-P | 0.24 | 0.56 | - | 64 | - |

[a] Based on ICP analysis; [b] based on $N_2O$ chemisorption; [c] based on $N_2$ physisorption; [d] based on TGA analysis under $H_2$

A series of catalysts were synthesized by one step sol-gel method. Different contents of Cu (4-25 wt%), Zn (15-63 wt%) and Al (0-23 wt%) (Table S1, entries 1-6), and Cu/Zn and Al/Zn ratios in the range of 0.08-1.18 and 0.47-3.68 (Table 1), respectively, were studied in order to evaluate the optimal composition. Interestingly, all experimental Cu values were close to the nominal values (5, 10, 20 or 25 wt%) (entries 1-6, Table 1). The low carbon (< 0.4 wt%) and nitrogen (< 0.05 wt%) contents of the catalysts confirmed that the calcination step at 400 °C was sufficient to remove the polyacrylic acid present during the syntheses, in agreement with our previously reported results on ZnO and Cu/ZnO synthesized by sol-gel method.[46]

As a representative example, the XRD diffractograms associated with the synthesis process of 25Cu-16Al-S1 after hydrolysis, calcination and reduction are presented in Figure 2. After hydrolysis, the structure is mainly amorphous. The peaks at 36.4°, 42.3° and 61.3° can be attributed to cubic $Cu_2O$ (▲, Pn-3m, PDF 00-005-0667) with a mean crystallite size of 34 nm. After calcination at 400 °C, the material presents mainly a crystalline monoclinic CuO structure (◇, C2/c, PDF 00-045-0937) with the main peaks at 35.3° and 38.4°. The peaks at 31.8° and 36.3° are associated with hexagonal ZnO (●, P63mc, PDF 01-079-0205). After reduction at 350 °C, CuO is reduced to cubic Cu (★, Fm-3m, PDF 04-13-9963), with peaks at 43.3°, 50.4 and 74.1°. ZnO is still present, but some crystalline cubic $ZnAl_2O_4$ (□, Fd-3m, PDF 04-014-1594) can also be observed, with the main contribution at 31.2° and 36.8°.

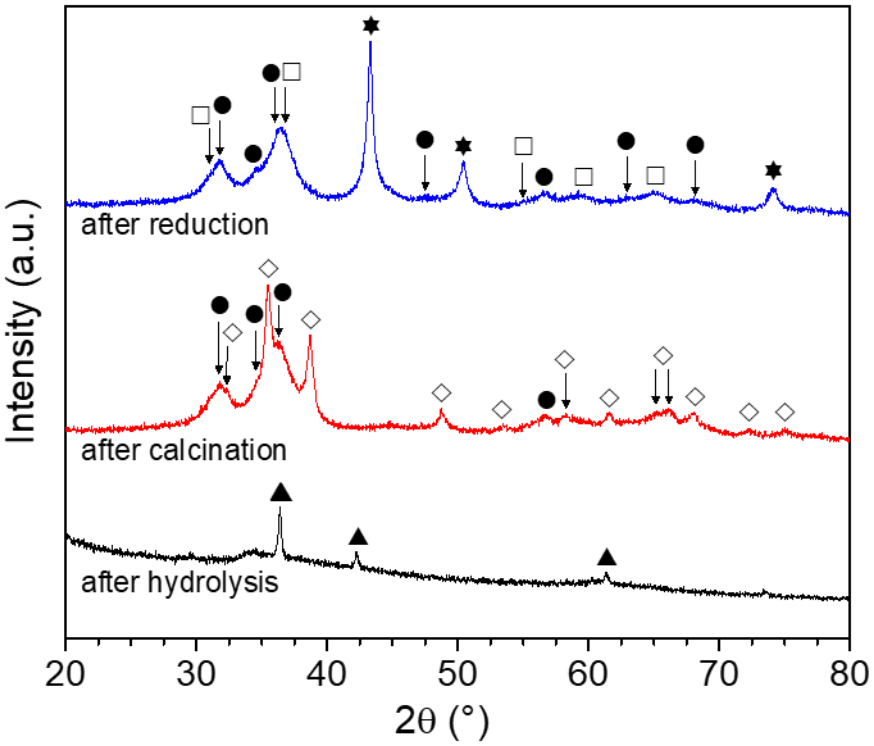


***Figure 2.*** *XRD diffractograms associated with 25Cu-16Al-S1 i) after hydrolysis, ii) after calcination at 400 °C and iii) reduction at 350 °C and passivation. Symbols refer to peaks*

*associated with (▲) $Cu_2O$ (Pn-3m, PDF 00-005-0667), (●) ZnO (P63mc, PDF 01-079-0205), (◇) CuO structure (C2/c, PDF 00-045-0937), (□) $ZnAl_2O_4$ (Fd-3m, PDF 04-014-1594) and (✸) Cu (Fm-3m, PDF 04-13-9963).*

The XRD diffractograms associated with the catalysts synthesized in one step (after reduction and passivation) are included in Figure 3. The Cu mean crystallite sizes of Cu-$Zn_xAl_yO$ are in the range of 4-13 nm (Table S1), for all the catalysts synthesized by sol-gel method with polyacrylic acid. The peaks associated with CuO are not detected, which suggest full reduction of the copper phase. The presence of $Cu_3Zn$ has previously been reported for Cu/ZnO[47] however we did not observe it for any of the catalysts. The lattice parameters associated with Cu were in the range of 3.614-3.625 Å, which is consistent with values for pure copper metallic phase reported in database PDF4+ (a = 3.607-3.625 Å). The crystallite size increases from 4 to 13 nm when the Cu content increases from ca. 4 to 25 wt%. The presence of Al has a strong impact on the crystallinity of the samples. Indeed, the diffractogram associated with Cu/ZnO (21Cu-S1) exhibits sharp ZnO peaks, leading to $d_{ZnO}$ around 20 nm, associated with large crystallites of Cu ($d_{Cu}$ = 16 nm, Table S1). While in presence of Al, the crystallite size of ZnO decreases (from 5 to 2 nm) when Al content ranges from 10 to 24 % and Al/Zn ratio increases from ca. 0.5 to 3.7 (Figure 4, Table S1). The peaks associated with $ZnAl_2O_4$ are small which suggest that the phase is predominantly amorphous. The formation of $CuAl_2O_4$ could not be ruled out as this phase exhibit a diffraction pattern similar to $ZnAl_2O_4$, however this phase is usually unstable below 600 °C.[48] Amorphous $Al_2O_3$ might also be present at high Al/Zn ratio. However, after calcination of a sample at 600 °C, $Al_2O_3$ was still not detectable and only crystalline $ZnAl_2O_4$ was observed in higher quantity (XRD not shown). When the synthesis was conducted without polyacrylic acid (11Cu-11Al-S1-P, Figure 3), large crystallites of Cu ($d_{Cu}$ = 36 nm) and ZnO ($d_{ZnO}$ = 13 nm) were formed which demonstrates the beneficial effect of polyacrylic acid during the sol-gel method.

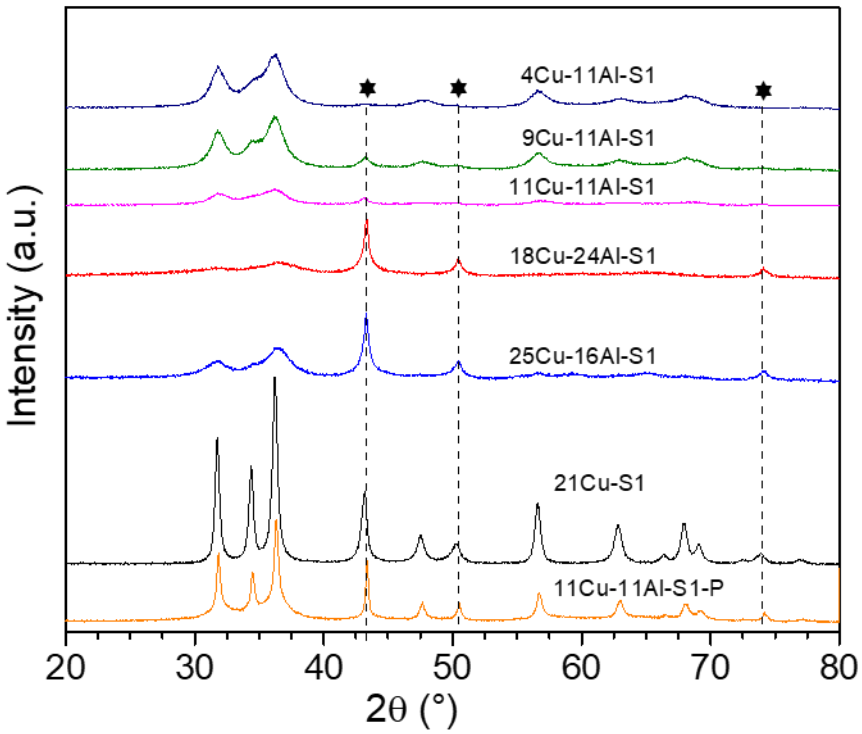

***Figure 3.*** *XRD diffractograms associated with 4Cu-11Al-S1, 9Cu-11Al-S1, 11Cu-11Al-S1, 18Cu-24Al-S1, 25Cu-16Al-S1, 21Cu-S1 and 11Cu-11Al-S1-P. Symbols (★) refer to Cu (Fm-3m, PDF 04-13-9963). The other peaks are associated with ZnO and* $ZnAl_2O_4$.

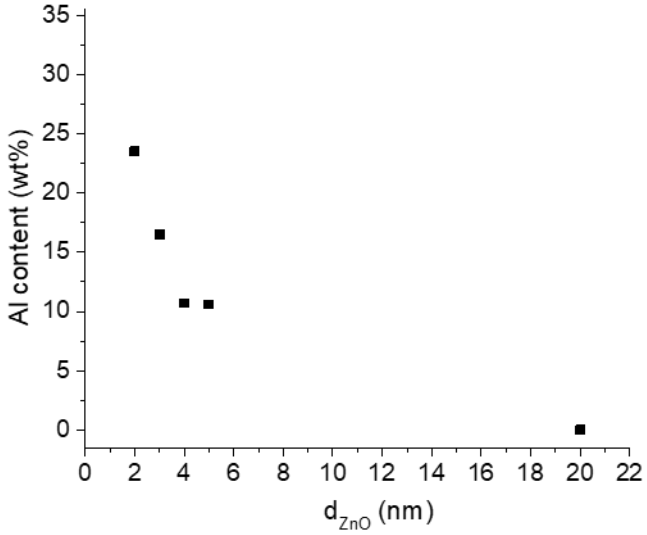


***Figure 4.*** *Effect of Al content on the main crystallite size of ZnO, for samples synthesized by S1 method.*

The catalyst without Al (21Cu-S1) exhibit low surface area (ca. 24 $m^2$ $g^{-1}$, Table 1). This result agrees with our previous study on ZnO synthesized by sol-gel method.[46] Indeed, despite high surface area after synthesis (up to 91 $m^2$ $g^{-1}$), the removal of polyacrylic acid after thermal treatment at 400 °C generated a collapse of the mesosphere associated with a low surface area. However, after incorporation of aluminum, surface areas up to 265 $m^2$ $g^{-1}$ were obtained despite the thermal treatment (Table 1). This value is higher than those previously reported in the literature for Cu-Zn-Al synthesized by co-precipitation (29-187 $m^2$ $g^{-1}$),[34–36,38] evaporation-induced self-assembly (79-225 $m^2$ $g^{-1}$),[41] oxalate gel co-precipitation (72-113 $m^2$ $g^{-1}$),[49,50] or sol-gel method (175 $m^2$ $g^{-1}$),[35] tested for the hydrogenolysis of glycerol.

The morphology of the samples was assessed by SEM. Pictures associated with the representative materials 11Cu-11Al-S1 and 18Cu-24Al-S1 are shown in Figure 5. The later sample, which displays a larger specific surface, is accompanied by a rougher structure (Figure 5b). The stoichiometries of the samples determined by EDX were in good agreement with the ICP analyses and confirmed a good homogeneity of the samples (Table S2).

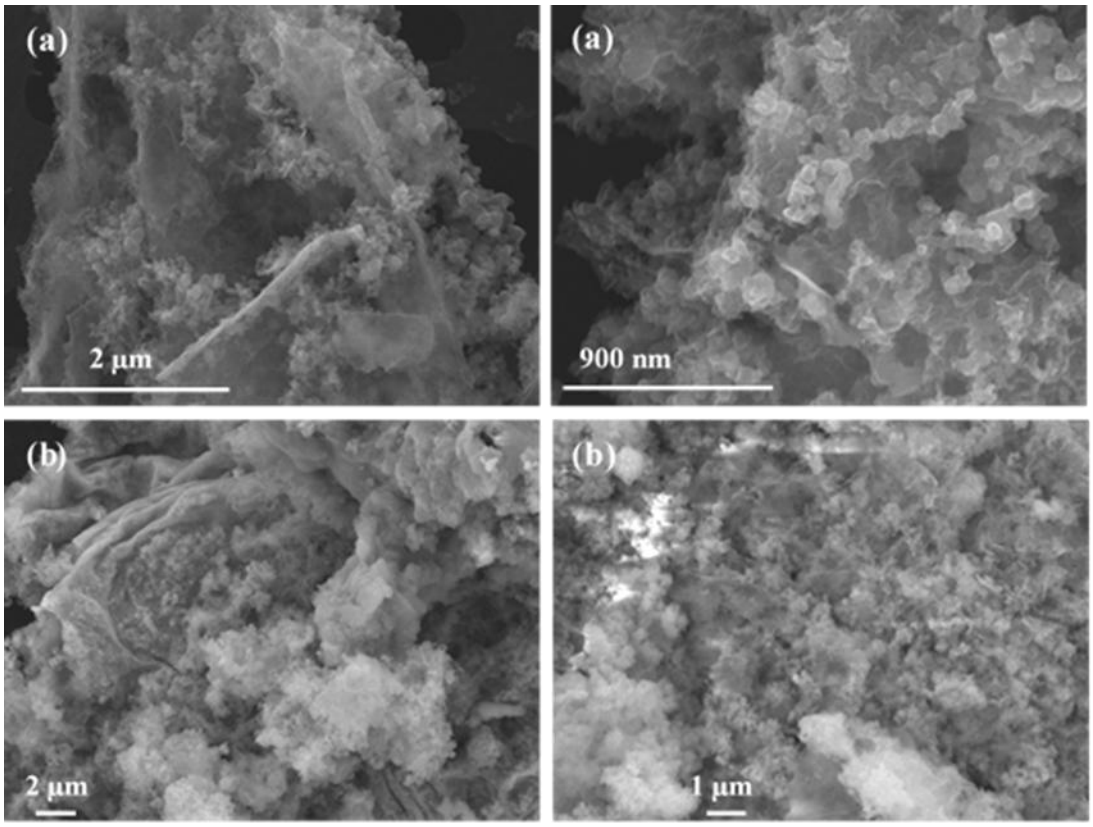


***Figure 5.*** *Representative SEM images associated with (a) 11Cu-11Al-S1 and (b) 18Cu-24Al-S1.*

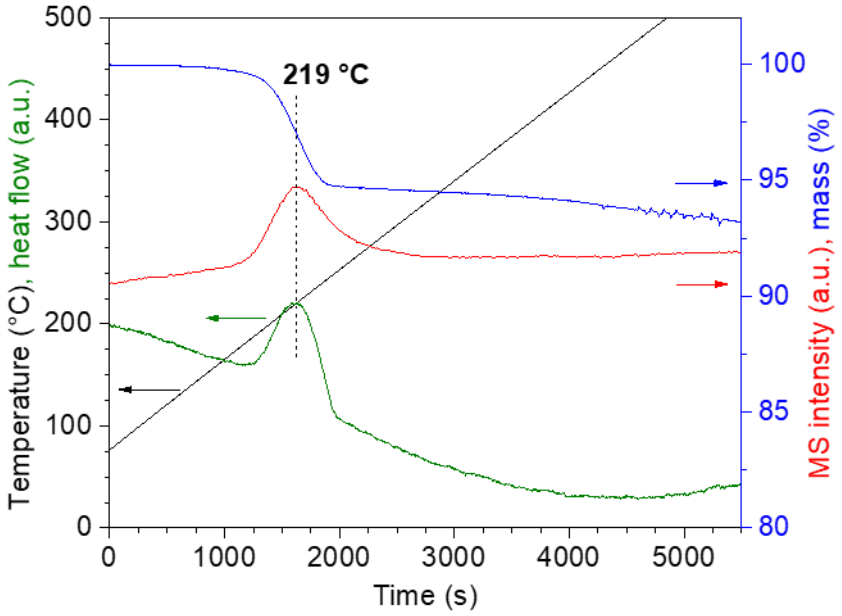


***Figure 6.*** *Evolution of mass (%), temperature (°C) and heat flow (a.u.) during TGA (5 °C min$^{-1}$) under 3% v/v $H_2$/Ar and associated $H_2O$ MS signal (m/z = 18) for 21Cu-S1.*

In order to assess the metal-oxide interaction, TGA analysis under 3% v/v $H_2$/Ar flow coupled to MS analysis were conducted on the materials after calcination. The profile associated with 21Cu-S1 is presented in Figure 6. The mass spectrum of the evolved gas was recorded and the only signals observed were at *m/z* = 17 and 18, which correspond to the formation of water caused by reduction of CuO to Cu. The peak at 219 °C observed with the MS is consistent with the mass loss and the endothermic signal of the heat flow. The temperature of reduction of the materials are included in Table 1, and the TGA profiles are presented in Figure S1. The temperatures of reductions (230-250 °C) are consistent with the values reported in the literature for Cu-Zn-Al systems (250-285 °C).[35,41,42] For these systems, the temperature of reduction depends mainly on the Cu content, the Cu crystallite size and the metal-oxide interaction which is linked to the method of preparation, the structure and morphology of the oxides, and the Al/Zn content.[35,41,48,50] It seems that at similar Al content (11Al-S1; entries 1-3 Table 1), the temperature of reduction increases with Cu content and particle size. The lower temperature of reduction for 21Cu-S1 suggest that when the nanoparticles of copper are dispersed on ZnO, the interaction between Cu and the support is weak. In presence of Al, Cu particles might be dispersed on the amorphous $ZnAl_2O_4$ phase and the interaction is stronger.

The specific Cu surface area of the catalysts were determined based on $N_2O$ chemisorption. After reduction *in situ* at 350 °C under $H_2$, the analyses were conducted at 90 °C. The gas flow is switched to $N_2O$/Ar/He and the MS signals of He, Ar, $N_2O$ and $N_2$ are recorded. A representative example of the experiment is presented in Figure S2. $N_2O$ is consumed and $N_2$ is formed due to the oxidation of Cu atoms at the surface of nanoparticles. The slight increase in temperature, from 90.0 °C to 90.6 °C, prove that this process is exothermic. No $N_2O$ was chemisorbed during a second passage of $N_2O$/Ar/He which confirms the complete oxidation during the first run. The specific Cu surface area ($Cu_{exp}$, $m^2_{Cu}$ $g^{-1}_{Cu}$, Table S1) and the concentration of accessible Cu sites ($Cu_s$, µmol $g^{-1}$, Table 1) of the materials were then determined based on $N_2O$ chemisorbed, with a stoichiometry of $Cu_s$:O estimated to be 2:1.[51] Mean particles sizes can be calculated from $N_2O$ chemisorption ($d_{Cu}$, $N_2O$) and are reported in Table S1. For all the catalysts with Al, the particles sizes are consistent with the crystallite sizes obtained by XRD (Table S1). However, for the catalyst without Al, there is some noticeable difference. This suggest that there is agglomeration of the Cu crystallites, hence a decrease in metal dispersion (due to the low BET surface area) along with a drop in active sites (i.e. concentration of accessible Cu sites).

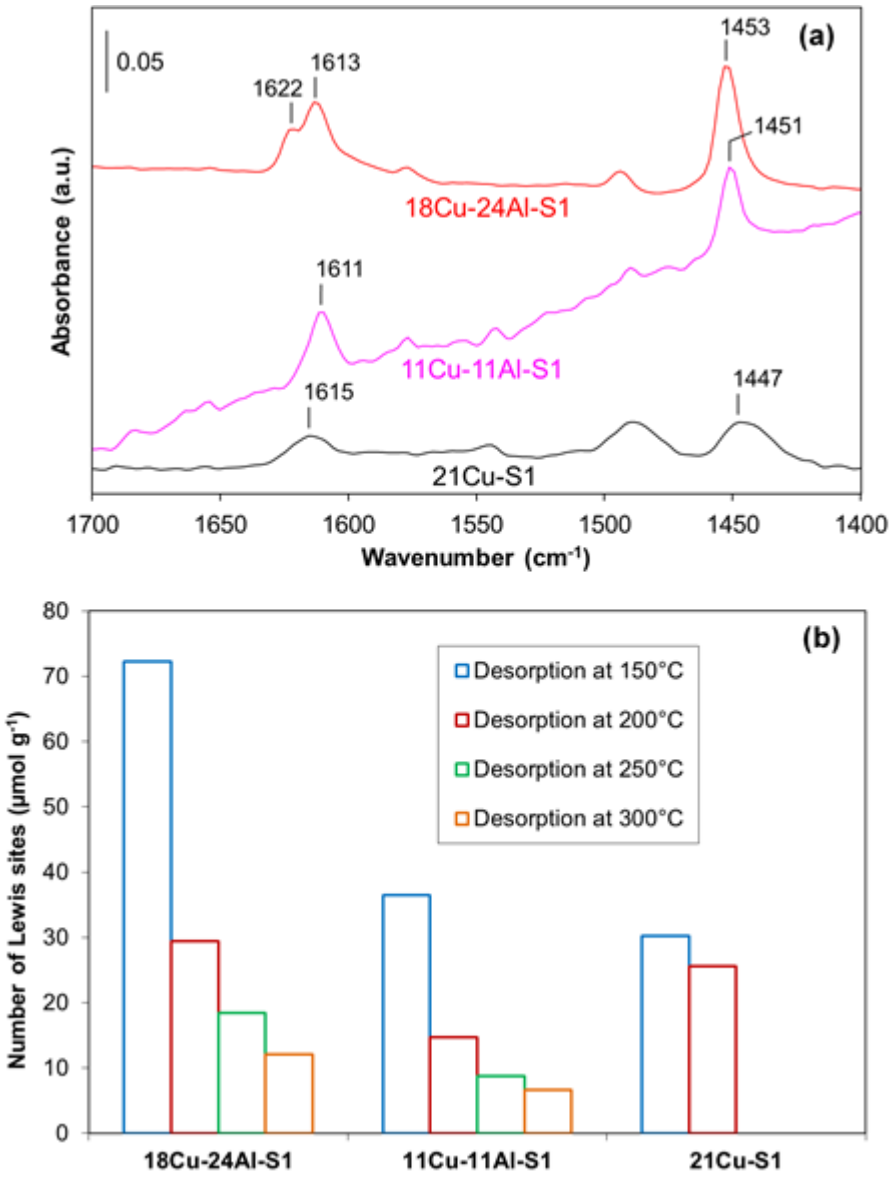


***Figure 7.*** *(a) FTIR spectra of pyridine adsorbed following outgas treatment at 150 °C and (b) total amount of Lewis sites after desorption at 150 °C, 200 °C, 250 °C, 300 °C, for 18Cu-24Al-S1, 11Cu-11Al-S1, and 21Cu-S1.*

FTIR analysis using pyridine as an established probe molecule was employed to investigate the surface acidity. The interaction of the nitrogen lone pair of the pyridine with Lewis acid sites on alumina and aluminates is associated with $\nu_{8a}$ and $\nu_{19b}$ bands whom the positions are in the range 1580–1625 $cm^{-1}$ and 1445–1455 $cm^{-1}$, respectively, where a higher frequency reflects stronger acidity.[52,53] The IR spectra of 18Cu-24Al-S1, 11Cu-11Al-S1 and 21Cu-S1 following outgas at 150 °C and their Lewis acid site concentrations are presented in Figure 7. The IR spectra following outgas at 200, 250, and 300 °C are shown in Figure S3. According to Figure 7a, the three catalysts exhibit two principal peaks at 1613 (± 2) $cm^{-1}$ and 1450 (± 3) $cm^{-1}$. After desorption at higher temperature (Figure S3), a higher frequency band

at 1620 (± 2) $cm^{-1}$ becomes predominant. The position of the first one is associated with relatively weak Lewis acidity associated to pyridine coordinated mainly to $Zn^{2+}$ in zinc aluminate structure.[54] However, Pyridine coordination to $Zn^{2+}$ in ZnO or $Al^{3+}$ sites cannot be ruled out. Indeed, in a first hand, pyridine adsorption on ZnO induce a band at 1605-1610 $cm^{-1}$ which fully disappears after desorption at 130 °C.[55,56] In addition, the sample Cu/ZnO (21 Cu-S1) present a broad band at 1615 $cm^{-1}$. In an other hand, in our desorption condition, pyridine on coordinatively unsaturated $Al^{3+}$ in octahedral sites should give a band at 1614-1617 $cm^{-1}$ [57–59] i.e. close to the position observed after evacuation at temperature higher than 150 °C. In the specific case of 18Cu-24Al-S1, Figure 7a evidenced a band at 1622 $cm^{-1}$ that can be attributed to pyridine adsorbed on strong Lewis acid sites (i.e. coordinatively unsaturated $Al^{3+}$ in tetrahedral sites). Finally, Figure 7a does not evidence the presence of Brønsted acid sites (characterized by a band at *ca.* 1540 $cm^{-1}$) which is consistent with previous reports on $ZnAl_2O_4$.[54,60]

Quantification of Lewis acid sites (Figure 7b) shows an increase of the total acid site concentration in the order 18Cu-24Al-S1 > 11Cu-11Al-S1 > 21Cu-S1. Therefore, the number of acid sites on the catalysts is directly linked to the Al content and formation of $ZnAl_2O_4$. While the acidity of Cu-ZnO[12,33,36] and Cu-Zn-Al[34] catalysts have been assessed by temperature-programmed desorption of ammonia, we could not find any other report in the literature dealing with the hydrogenolysis of glycerol that provides measure of acidity of Cu-Zn-Al catalysts by FTIR analysis with pyridine.

**Synthesis and characterization of the catalysts synthesized by two steps method**

For comparison, two supports with two different Al contents were synthesized by sol-gel method in two steps. The Al and Zn contents of the supports were consistent with the theoretical loadings and Al/Zn ratios of 0.5 and 2.5 were obtained (Table 2 and Table S1).

**Table 2.** Main textural and structural properties of $Cu/ZnAl_xO_y$ synthesized in two steps

| Catalysts | $n_{Cu}/n_{Zn}$ [a] | $n_{Al}/n_{Zn}$ [a] | $Cu_s$ ($\mu mol_{Cu}\ g^{-1}$) [b] | Surface area ($m^2\ g^{-1}$) [c] | $T_{reduction}$ (°C) [d] |
|---|---|---|---|---|---|
| 11Al | - | 0.51 | - | 71 | - |
| 26Cu/11Al-S2 | 0.72 | 0.75 | 322 | 111 | 250 |
| 22Al | - | 2.47 | - | 223 | - |
| 16Cu/22Al-S2 | 0.76 | 2.41 | 210 | 167 | 250 |

[a] Based on ICP analysis; [b]based on $N_2O$ chemisorption; [c]based on $N_2$ physisorption; [d]based on TGA analysis under $H_2$

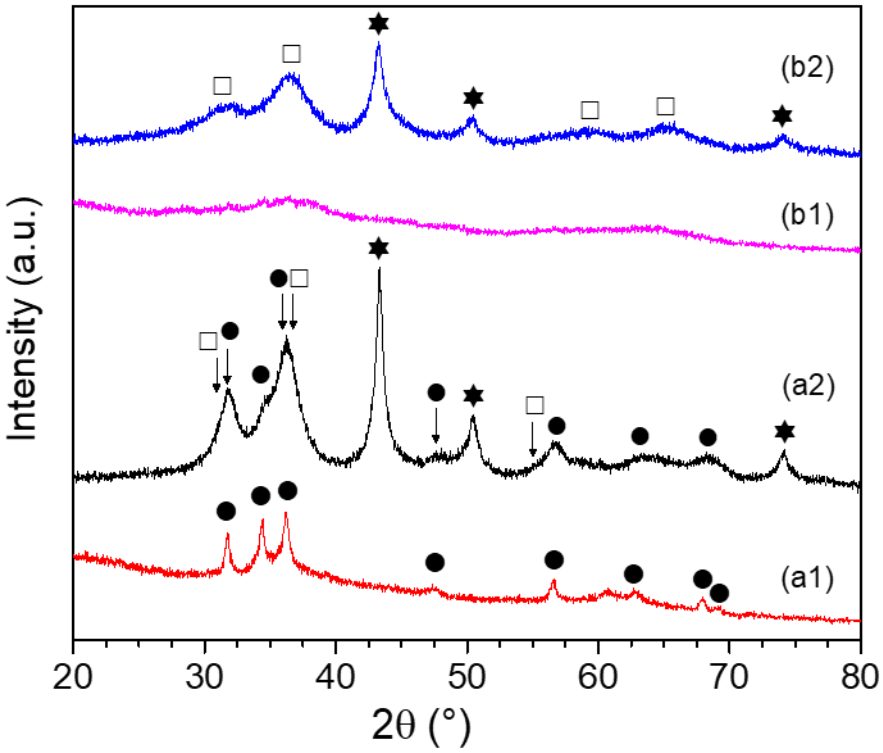


***Figure 8.*** *XRD diffractograms associated with (a1) 11Al, (a2) 26Cu/11Al-S2, (b1) 22Al and (b2) 16Cu/22Al-S2. Symbols refer to peaks associated with (●) ZnO (P63mc, PDF 01-079-0205), (□) $ZnAl_2O_4$ (Fd-3m, PDF 04-014-1594) and (✸) Cu (Fm-3m, PDF 04-13-9963).*

For low Al content, 11Al support exhibits a ZnO crystalline phase (Figure 8-a1), associated with a relatively low surface area (71 $m^2$ $g^{-1}$, Table 2). As the support did not undergo any thermal treatment after synthesis, an amorphous zinc aluminate phase might also be present. At higher Al content, 22Al is amorphous (Figure 8-b1) and the material displays a much higher surface area (223 $m^2$ $g^{-1}$, Table 2). The copper was then added by deposition-precipitation with urea, followed by calcination, reduction and passivation. The XRD diffractograms (Figure 8) showed that the catalyst 26Cu/11Al-S2 exhibit relatively dispersed Cu particles ($d_{Cu}$ = 9 nm, Table S1) on a support composed of crystalline ZnO. The zinc aluminate must be principally amorphous, as the peaks associated with crystalline $ZnAl_2O_4$ (□) are small (Figure 8-a2). The metal contents of the catalysts were measured by ICP and compared to the ones of the support after calcination at 400 °C, i.e. after similar heat treatment. The results included in Table S1 show a major difference between 11Al and 26Cu/11Al-S2, since the final Zn content was lower than the expected one (37% vs. 48%). This suggest that ZnO is not really stable in the conditions employed for the deposition-precipitation (water, pH ≈ 8, 60 °C) and dissolved during the synthesis. This phenomenon was confirmed by ICP analysis of the solution after filtration which showed the presence of $Zn^{2+}$. This demonstrates the beneficial effect of the one pot sol-gel method in presence of polyacrylic acid, for the catalysts with low Al contents. This problem does not occur for

16Cu/22Al-S2 which exhibits the expected metal loading (Zn, Al, Cu). This could be attributed to the sole presence of amorphous $ZnAl_2O_4$ which is more stable in aqueous phase. After thermal treatment, the catalyst 16Cu/22Al-S2 exhibits a crystalline $ZnAl_2O_4$ phase. The surface area, $T_{reduction}$ and $Cu_s$ (Table 2) are in the range of the values obtained for $Cu/ZnAl_xO_y$-S1 synthesized in one pot. However, the particle size obtained by $N_2O$ chemisorption are slightly higher than those obtained by XRD, suggesting a lower dispersion of the Cu nanoparticles. It is worth noting that compared to syntheses without Al which gave catalysts with specific surface areas of 20-30 $m^2\ g^{-1}$,[46] the addition of aluminium significantly increased those of the support and the final catalyst. Representative SEM images of the catalysts are shown in Figure S4. The catalyst 16Cu/22Al-S2 exhibits platelet-like structure, while 26Cu/11Al-S2 presents agglomerates of flake-like particles.

## Hydrogenolysis of glycerol over $Cu/ZnAl_xO_y$

**Table 3.** Conversion and selectivity to 1,2-propanediol for the hydrogenolysis of glycerol

| Entry | Catalysts | Conversion (%) | $S_{PDO}$ (%) |
|---|---|---|---|
| 1 | 4Cu-11Al-S1 | 21 | 97 |
| 2 | 9Cu-11Al-S1 | 52 | 86 |
| 3 | 11Cu-11Al-S1 | 74 | 83 |
| 4 | 18Cu-24Al-S1 | 79 | 85 |
| 5 | 25Cu-16Al-S1 | 96 | 83 |
| 6 | 21Cu-S1 | 40 | 89 |
| 7 | 11Cu-11Al-S1-P | 45 | 91 |
| 8 | 26Cu/11Al-S2 | 93 | 78 |
| 9 | 16Cu/22Al-S2 | 44 | 91 |

Results after 24 h, with 500 mg of catalyst; 100 mL of 0.23 M glycerol in water; 200 °C and 30 bar of $H_2$

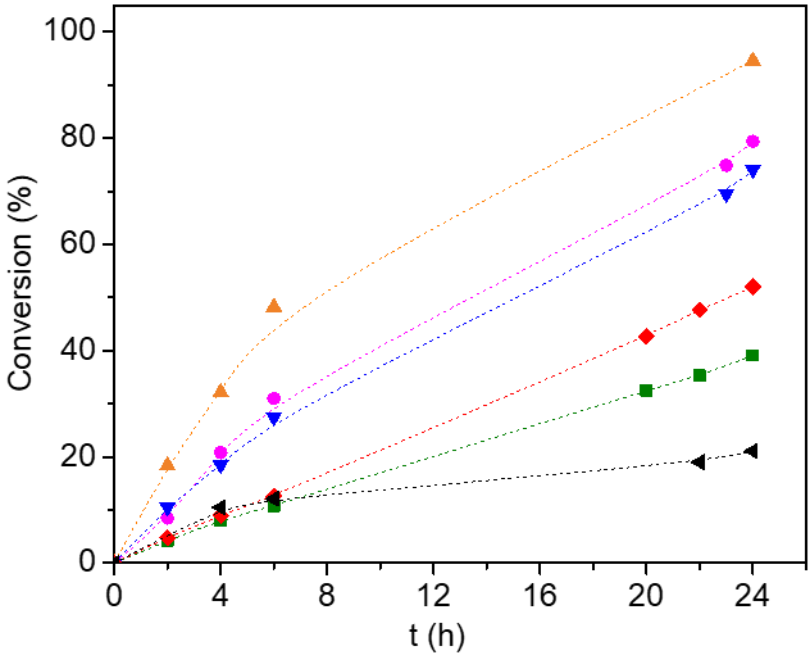


***Figure 9.*** *Temporal evolution of the conversion of glycerol (%) for the catalysts synthesized by S1 method: (▲) 25Cu-16Al-S1 (●)18Cu-24Al-S1 (▼) 11Cu-11Al-S1 (◆) 9Cu-11Al-S1 (■)21Cu-S1 (◀) 4Cu-11Al-S1. Aqueous solution of glycerol (100 mL of 0.23 M glycerol in water; 500 mg of catalyst, 200 °C and 30 bar of $H_2$).*

The hydrogenolysis of glycerol was studied over all the catalysts in a batch reactor at 200 °C, under 30 bar of $H_2$. The temporal evolution of the conversion of glycerol observed over 24 h, with the catalysts synthesized by S1 method are included in Figure 9. Those associated with the other catalysts are shown in Figure S5. Glycerol was converted to 1,2-propanediol as major product and ethylene glycol as secondary product (Scheme S1). 1,3-propanediol was not detected, suggesting a higher reactivity of the primary than secondary hydroxyl group, which might be due to less steric hindrance.[61] The further hydrogenolysis of the diols to monoalcohols (i.e. propanol, ethanol) did not occur. The conversion and the selectivity to 1,2-propanediol ($S_{PDO}$) after 24 h are included in Table 3. For all the reactions, the carbon balance was always above 95%. The selectivity towards 1,2-propanediol is high (≥ 95%) at low conversion (≤ 20%) and decreases slowly (down to ≈ 80%) with increasing conversion, in favor of ethylene glycol. The selectivity is directly correlated to the conversion (Figure 10) and does not depend on the catalysts or time.

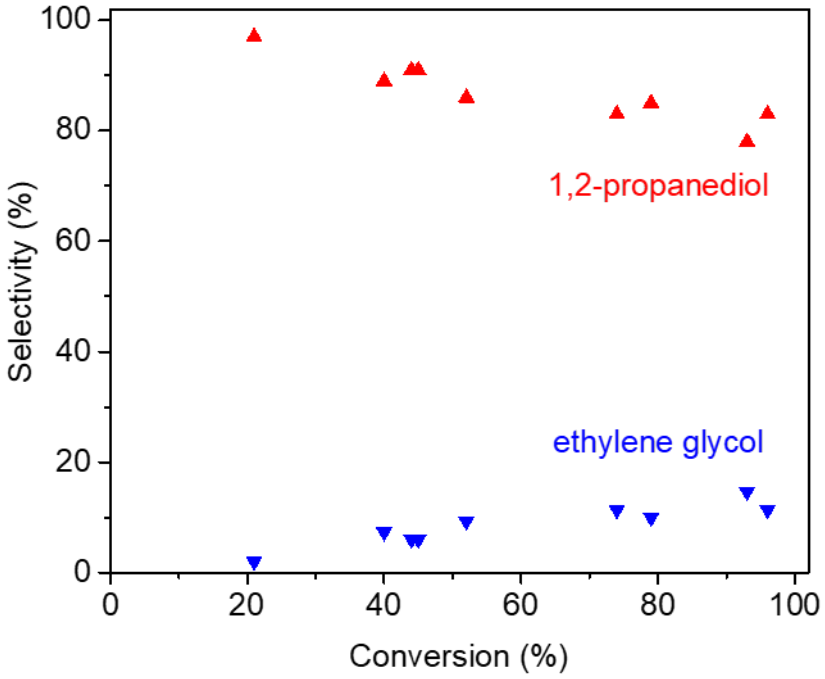


***Figure 10.*** *Selectivity towards 1,2-propanediol (▲) and ethylene glycol (▼) as function of glycerol conversion, obtained over all the catalysts (after 24 h). Aqueous solution of glycerol (100 mL of 0.23 M glycerol in water; 500 mg of catalyst, 200 °C and 30 bar of $H_2$).*

It is well accepted that on Cu catalysts (Cu/ZnO[11], Cu/$ZrO_2$[23,24], Cu/$Al_2O_3$[14,14], Cu/AlO(OH)[62], Cu/ZnO/$Al_2O_3$[63]) the dehydration of glycerol on acid sites can generate the acetol which is then hydrogenated on the metallic sites to 1,2-propanediol. This pathway has been shown to be favored in presence of Lewis acid sites originating mainly from the supports,[14,38,62] but also from metal sites[64,65]. On the contrary, Brønsted acid sites favor the formation of 1,3-propanediol and lower alcohols.[64,66,67] It is well known that the presence of water can partially hydroxylate the surface.[68] The formation of OH groups poison the Lewis acid sites and inhibit dehydration reactions.[69] Moreover it has also been reported on $Al_2O_3$ that water can promote the formation of (Al,O) Lewis acid-base pair; thus, increasing the basicity of neighboring oxygens can enhance the catalytic activity.[70,71] However, we did not observe any 1,3-propanediol which suggests that this phenomenon hardly occurs. The formation of ethylene glycol is believed to occur through dehydrogenation of glycerol to glyceraldehyde, followed by direct decarbonylation.[72] The formation of ethylene glycol through retro-aldol condensation of glyceraldehyde followed by hydrogenation has also been reported,[72] however it would be associated with the formation of methanol, which was not observed under our conditions.

The performances of the catalysts may be documented by different values: The amount of glycerol converted in 24 h, per mol of Cu (Cu efficiency, $n_{gly}/n_{Cu}$) or per mass of catalyst (productivity, $n_{gly}/m_{catalyst}$, $mmol_{gly}\ g^{-1}$) and the initial rates ($V_0$, $mmol_{gly}\ g_{Cu}^{-1}\ h^{-1}$) are included in Table S3. The dehydration of glycerol is favored on Lewis acid sites and generates the acetol,

as a first step. We did not observe any acetol intermediate during the reaction when working under $H_2$ which suggest that the dehydration is not the limiting step; one reaction was conducted with Cu-ZnO under Ar in order to confirm the formation of acetol as intermediate. Moreover, there is no clear correlation between the productivity and the Al content, i.e. Lewis acidity, suggesting partial blockage of Lewis acid sites due to the water. The results obtained over the catalysts synthesized by S1 show that the conversion increases, from 21% to 96%, when increasing the Cu loading, from 4 to 25% (Table 3, entry 1 to 5). This suggest that the activity is correlated to the metallic sites, which favor the hydrogenation step. Despite the increase in conversion with the Cu loading, the Cu efficiency varied between 5 and 20 $mol_{gly}$ $mol_{Cu}^{-1}$ and the initial rates ranged from 4 to 28 $mmol_{gly}$ $g_{Cu}^{-1}$ $h^{-1}$, i.e. there is no clear trend associated with Cu efficiency and initial rates (Table S3). For example, without Al, the catalyst 21Cu-S1 (entry 6) is far less active than 18Cu-24Al-S1 with similar Cu loading (entry 4). This suggest that the Cu loading is not the only parameter contributing to the activity. The conversion observed for 11Cu-11Al-S1-P (entry 7) is much lower (45%) than for 11Cu-11Al-S1 (entry 3, 74%), which proves the crucial role of polyacrylic acid during the synthesis.

We then focused on the productivity of the catalyst ($n_{gly}/m_{catalyst}$) in function of the concentration of accessible Cu sites ($Cu_s$) where a clear correlation is observed (Figure 11). This is consistent with previous literature on the hydrogenolysis of glycerol to 1,2-propanediol over Cu/ZnO[9,37], $Cu/SiO_2$[18,19] and $Cu/ZrO_2$[23]. The concentration of active sites is correlated to the Cu loading and particle size. This also explains the lower conversion observed with 21Cu-S1 as the main particle size obtained by $N_2O$ chemisorption is large (46 nm). The beneficial effect of Al seems to be associated with the larger surface area of the catalysts and the stronger metal-oxide interaction, which favor a better dispersion of the copper, i.e. an increase of the concentration of accessible metallic sites. Similarly, in the absence of polyacrylic acid during the synthesis, large particles of Cu were obtained, which generated a low conversion. One catalyst does not fit perfectly the trend, namely 4Cu-11Al-S1. Indeed, while its initial rate is quite high, it seems to deactivate quickly, so the productivity of the catalyst ($n_{gly}/m_{catalyst}$) is low. This might be due to the weak metal-oxide interaction observed with this catalyst (i.e. low temperature of reduction, Table 1) and small crystallite size which favor sintering and problem of stability during the reaction. It is interesting to note that the two catalysts synthesized in two steps fits perfectly the trend (Figure 11). 26Cu/11Al-S2 exhibits similar Cu efficiency and productivity as 25Cu-16AlS1.

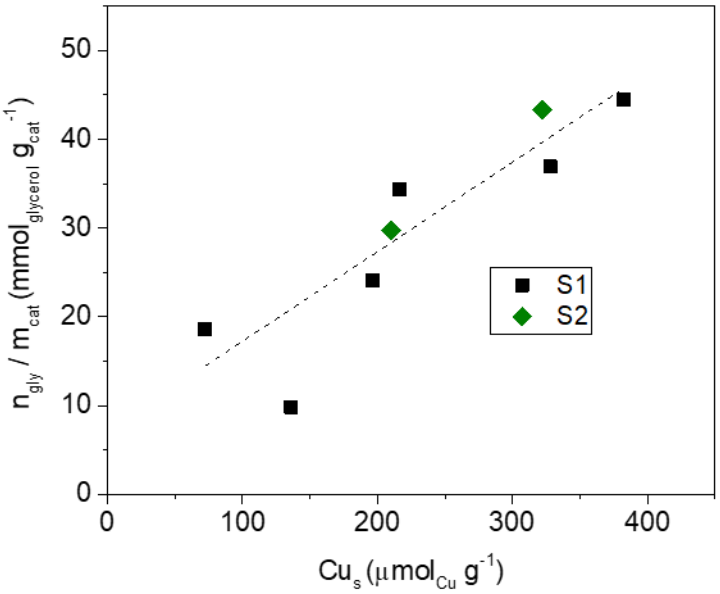


***Figure 11.*** *Productivity of the catalysts ($n_{gly}$ / $m_{catalyst}$) in function of the total number of active sites, for the catalysts synthesized by S1 (!) and S2 (Λ) methods. Aqueous solution of glycerol (100 mL of 0.23 M glycerol in water; 500 mg of catalyst, 200 °C and 30 bar of $H_2$).*

To conclude, the activity of the catalysts is directly linked to the concentration of accessible Cu active sites. Moreover, the presence of polyacrylic and Al is crucial for the formation of $ZnAl_2O_4$ along with small Cu particles, which favor the conversion of glycerol to 1,2-propanediol.

Our productivity results obtained are competitive compared to the best literature values reported for non-noble metal catalysts. The difficulty in the interpretation of these data lies in the variation of the parameters, such as pressure, temperature and the lack of quantification of active sites for some studies. However it is worth noting that the literature focused on the hydrogenolysis of aqueous glycerol over Cu supported on oxides report conversion below 80%, when working under similar reaction conditions (T = 180–200 °C, $P_{H2}$ = 20–80 bar, batch reactor).[73] Moreover, our best catalyst generated yields up to 80 % of 1-2-propanediol, which is similar to the highest values reported for other Cu-Zn-Al systems (76-85 %).[41,42,50]

**Stability and recyclability of the catalysts**

The stability of catalyst is a crucial criterion for industrial application. For the hydrogenolysis of glycerol in liquid phase, it has been shown that deactivation of non-noble catalysts usually occurs and a number of factors have been proposed. For Cu catalysts, the deactivation has been principally attributed to metal sintering.[12,19,23,30,33,38,41,42] This phenomenon is usually linked to a change in morphology of the solid from spherical particles to lamellar or rod-like structure, associated with an increase in crystallite size and a decrease in surface area and pore volumes of the material.[12,19,33,34] It has also been shown that the use of water as solvent emphasis particles agglomeration.[33,42]

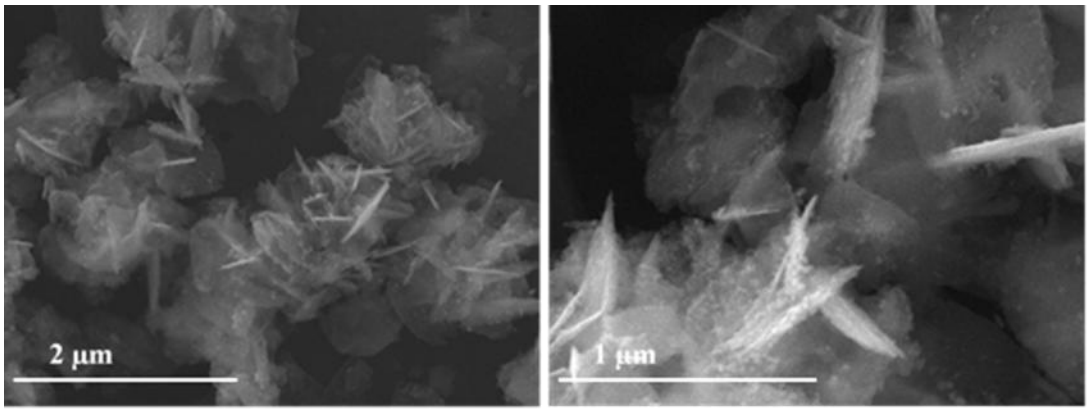


***Figure 12.*** *Representative SEM image associated with 11Cu-11Al-S1 after reaction.*

The catalysts exhibiting the highest Cu efficiency (11Cu-11Al-S1) and productivity (25Cu-16Al-S1, 26Cu/11Al-S2) were characterized after reaction and compared to 21Cu-S1. Figure S6 presents the XRD diffractograms associated with these catalysts after 24 h reaction. In agreement with the literature, all the catalysts exhibit larger Cu crystallite size (Table S4). Moreover, the three catalysts present the formation a new phase corresponding to monoclinic $Zn_5(CO_3)_2(OH)_6$, with a characteristic peak at 12.9°. We previously demonstrated for Cu/ZnO[46] that this carbonic phase appeared only at high conversion (> 60 %) and was associated with the formation of products resulting from C-C bond cleavage. This phase was not observed for 21Cu-S1 due to the lower conversion (40 %). SEM images of 11Cu-11Al-S1 (Figure 12) shows a change in morphology with the formation of a lamellar structure due to the formation of the hydrozincite phase. It is worth noting that this change of structure of the solids is also associated with a drastic increase in surface area after reaction for $Cu/Zn_xAl_yO$-S1 (from 80-100 $m^2\ g^{-1}$ to *ca.* 145 $m^2\ g^{-1}$) while it remained stable for $Cu/Zn_xAl_yO$-S2 (ca. 110 $m^2\ g^{-1}$) and Cu/ZnO (ca. 25 $m^2\ g^{-1}$; Table S4). The solutions after 24 h reaction were analyzed by ICP in order to assess any metal leaching. In line with the literature,[19,34,38] no Cu or Al were lost during the hydrogenolysis of glycerol, however small quantities of Zn were found (10-15 % wt.; Table S4). The stability of ZnO under hydrothermal conditions is limited, so it might solubilize and reprecipitate, which might favor the formation of carbonates species such as $Zn_5(CO_3)_2(OH)_6$.

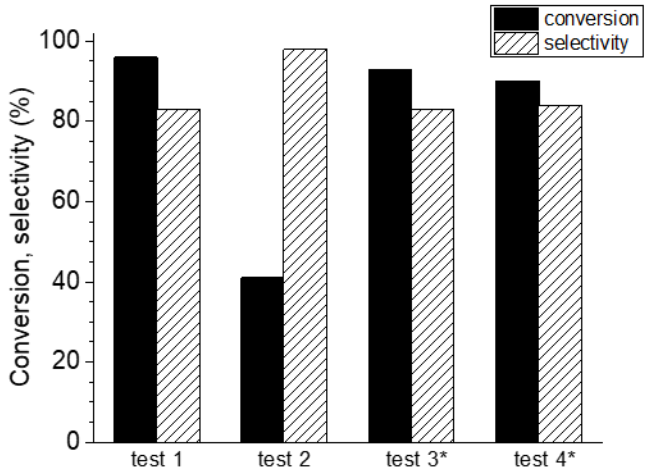


***Figure 13.*** *Recyclability of 25Cu-16Al-S1. The catalyst was re-activated under $H_2$ at 350 °C before test 3 and test 4.*

***Table 4.*** *Surface area and $d_{Cu}$ for 25Cu-16Al-S1 after syntheses and after recycling*

| **Catalyst** | **Surface area ($m^2$ $g^{-1}$)[a]** | **$d_{Cu}$ (nm)[b]** |
|---|---|---|
| Fresh | 97 | 12 |
| Test 1 | 142 | 18 |
| Test 2 | 149 | 18 |
| Test 3[c] | 150 | 20 |
| Test 4[c] | 155 | 21 |

[a]based on $N_2$ physisorption, [b]based on XRD analysis
[c]The catalyst was re-activated under $H_2$ at 350 °C before test 3 and test 4

The recyclability of 25Cu-16Al-S1 was assessed over 4 consecutive runs. Test 2 was conducted without regeneration, i.e. the catalyst was reused directly after filtration and drying at 80 °C. Unfortunately, the catalyst was far less active (Figure 13). This result suggests that the presence of $Zn_5(CO_3)_2(OH)_6$ must be detrimental for the activity. It could also be due to the formation of copper oxide during the recovery of the catalyst. In the literature,[41,42] the stability of Cu-Zn-Al systems are usually assessed after regeneration. Therefore, the catalyst was then reduced under $H_2$ before test 3 and before test 4. It is interesting to note that the surface area and the main Cu crystallite size remained stable from the second run (Table 4) and no Zn was lost (< 1 % wt.). The conversion of glycerol and selectivity to 1,2-propanediol remained stable after the 4° runs (Figure 13).

## Conclusion

In this study, we have elaborated Cu-Zn-Al systems based on sol-gel synthesis in presence of polyacrylic acid. This simple method can be conducted in one step. Catalysts with really high surface area, up to 265 $m^2$ $g^{-1}$, were obtained. The presence of aluminum and polyacrylic acid during syntheses favored the formation of small and well dispersed Cu nanoparticles, with a

mean size in the range of 4 to 13 nm. The acidity of the catalysts was assessed by FTIR analysis using pyridine. The catalysts exhibit Lewis acidity where the number of acid sites is correlated to the Al content. The hydrogenolysis of glycerol was studied in a batch reactor at 200 °C, under 30 bar of $H_2$. Glycerol was converted to 1,2-propanediol as major product and ethylene glycol as secondary product. Conversions of glycerol up to 96% were observed, with selectivity towards 1,2-propanediol around 80-90%. We demonstrated that the productivity of the catalyst was directly linked to the number of Cu active sites. Our results showed that the activity is correlated to the metallic sites, which favor the hydrogenation step and that the catalysts can be recycled several times after reactivation under $H_2$.

## Experimental Section

### Reagents

$ZnEt_2$ (15%wt in toluene), $[Al(CH_3)_3]_2$ (97%), $Cu(NO_3)_2.3H_2O$ (99.9%), glycerol (99.5%), urea (99%), ethanol (99.5%) and aqueous solutions of polyacrylic acid (50 wt%) of molecular weight of 2000 g $mol^{-1}$ were purchased from Merck and used as received.

### Catalysts preparation

### Two steps synthesis of $Cu/ZnAl_xO_y$

#### *Synthesis of $ZnAl_xO_y$ by Sol-Gel process (XAl)*

200 mL of an aqueous solution of polyacrylic acid (PAAH, molecular weight of 2000 g $mol^{-1}$) at 0.63 wt% was placed in a Schlenk flask of 500 mL. The solution was stirred at 1000 rpm under Ar. The flask was immerged in an ice bath for 30 min in order to reach the 0 °C desired temperature. In another Schlenk flask of 50 mL, between 3 and 12 mL of $[Al(CH_3)_3]_2$ (in regards to *x*) was added to 14.4 mL of $ZnEt_2$ solution in toluene under argon. The mixture of $[Al(CH_3)_3]_2$ and $ZnEt_2$ was then transferred slowly (under argon) to the aqueous solution of polyacrylic acid. Immediately after the transfer, ethane and methane gases were generated and evacuated by the bubbler connected to the 500 mL flask and a white precipitate appeared. After 1 h of stirring, the suspension was centrifuged at 8000 rpm for 30 min. 90 mL of ethanol was added to the wet powder obtained after centrifugation and the mixture was kept under stirring at room temperature for 30 min. Once again, the suspension was centrifuged at 8000 rpm for 30 min. The resulting white powder was dried in an oven at 80 °C for 20 h.

The samples will be labelled *X*Al, with *X* = Al content (wt%).

#### *Synthesis of $Cu/ZnAl_xO_y$ by deposition-precipitation process with urea (ACu/XAl-S2)*

1.8 g of the support (*X*Al) was suspended in 150 mL of distilled water, in a 500 mL flask and 4 g of urea (66 mmol) and the appropriate volume of an aqueous copper nitrate solution [$Cu(NO_3)_2 \cdot 3H_2O$, 0.157 M] were added to the support. The appropriate amount of distilled water was added to obtain a final $Cu^{2+}$ concentration of 20.8 mM. The suspension was heated at 1 °C $min^{-1}$ to 60 °C and hold for 3 h. The resulting solids were filtered and washed with 100 mL of distilled water. After drying at 100 °C for 20 h, the solids were calcined at 400 °C (5 °C $min^{-1}$; hold for 4 h) in a furnace. They were then reduced in a cell under 50 mL $min^{-1}$ of $H_2$ at 3 °C $min^{-1}$ up to 350 °C and hold for 1 h, and finally passivated for 30 min under 50 mL $min^{-1}$ of 1% v/v $O_2/N_2$ at room temperature.

The samples will be labelled *A*Cu/*X*Al-S2, with *A* = Cu content (wt%), *X* = Al content (wt%), and S2 referring to the two steps synthesis.

**One step Sol-Gel synthesis of Cu/$ZnAl_xO_y$ (*ACu-XAl-S1*)**

The same procedure as above (*Synthesis of $ZnAl_xO_y$ by Sol-Gel process)* was followed except that 4 g of urea (66 mmol) and the appropriate volume of an aqueous copper nitrate solution [$Cu(NO_3)_2 \cdot 3H_2O$, 0.157 M] were added from the start in the aqueous solution of polyacrylic acid. After stirring at 0 °C for 1 h, the solution was heated at 1 °C $min^{-1}$ to 60 °C and hold for 3 h. The resulting precipitates were filtered and washed with 100 mL of distilled water. After drying at 100 °C for 20 h, the solids were calcined at 400 °C (5 °C $min^{-1}$; hold for 4 h) in a furnace. They were then reduced in a cell under 50 mL $min^{-1}$ of $H_2$ at 3 °C $min^{-1}$ up to 350 °C and hold for 1 h, and finally passivated for 30 min under 50 mL $min^{-1}$ of 1% v/v $O_2/N_2$ at room temperature.

The samples will be labelled *A*Cu-*X*Al-S1, with *A* = Cu content (wt%), *X* = Al content (wt%) and S1 referring to the one step synthesis. For comparison, one sample was synthesized without polyacrylic acid, and labelled *A*Cu-*X*Al-S1-P.

**Characterization of catalysts**

Powder X-ray diffraction patterns (XRD) of the samples were recorded using a Bruker D8 Advance Diffractometer equipped with a nickel filter, a copper tube (λKα (Cu) = 1.54184 Å) and a multi-channel fast detector (LynxEye 192 channels an active length of 2.947 °). The samples were scanned at 0.04 ° $s^{-1}$ over the range $20 \leq 2\theta \leq 80°$. Phase identification was achieved using HighScore Plus and the JCPDS-ICDD-PDF4+ database. Mean crystallite sizes (± 0.5 nm) and lattice parameters (± 0.005 Å) were obtained by performing Rietveld refinements using Topas 5.

The Cu, Zn and Al contents (wt%) were determined by inductively coupled plasma optical emission spectroscopy (ICP-OES) by using an ACTIVA instrument (HORIBA Jobin Yvon). Before analysis, the solid samples were mineralized in an acid mixture and heated at 250-300 °C. Elemental analysis of light elements (CHN) was performed on an analyzer Thermo Fisher Flash 2000. The values are reported with an absolute accuracy of ± 0.1 %.

The surface areas of the samples (± 5 $m^2$ $g^{-1}$) were determined with the BET method from $N_2$ physisorption at -196 °C using an ASAP 2020 Micromeritics apparatus. Before the measurements, the materials were outgassed at 150 °C for 2 h under vacuum ($10^{-4}$ mbar). The specific surface area was calculated from the obtained isotherms for P/P° between 0.05 to 0.25. The values are reported with an absolute accuracy of ± 5 $m^2$ $g^{-1}$.

The thermogravimetric analyses (TGA) were performed on a SETARAM LABSYS instrument in the 25-650 °C temperature range, on ca. 20 mg of sample, with a heating rate of 5 °C $min^{-1}$, under air flow (50 mL $min^{-1}$). This technique was used to determine the optimal temperature of calcination. Simultaneous thermogravimetric and differential thermal analyses (TG-DTA) of the samples were conducted on a SETARAM SETSYS Evolution 12 thermo-analyzer coupled via a heated (*ca*. 150 °C) capillary with a Pfeiffer OmniStar quadrupole mass spectrometer (MS). For TG-DTA-MS studies, ca. 20 mg of samples were heated from

room temperature to 750 °C at a constant rate of 5 °C $min^{-1}$ under 3% v/v $H_2$/Ar (50 mL $min^{-1}$).

In order to reveal morphology of the materials, SEM images were obtained using ZEISS MERLIN COMPACT VP microscope with low-vacuum detector (SE) and Oxford 50 $mm^2$ EDX detector (12 analyses were conducted for each sample).

The specific Cu surface area ($Cu_{exp}$, ± 2 $m^2_{Cu}$ $g^{-1}_{Cu}$), the mean particles sizes ($d_{Cu,\ N2O}$, ± 0.5 nm) and the concentration of accessible Cu sites ($Cu_s$, ± 3 $\mu mol_{Cu}$ $g^{-1}$) of the materials were determined based on $N_2O$ chemisorption. Quantitative $N_2O$ adsorption measurements were made with a homemade analytical setup allowing to follow the change in the composition of the gas mixture at the outlet of a quartz micro reactor (≈ 1.5 mL) containing the pretreated catalyst (weight range of 0.2-0.3 g, deposited on quartz wool) by using a quadrupole mass spectrometer (Inficon, Transpector CPM). The temperature was recorded via a stainless-steel K type thermocoax (Φ= 0.25 mm) inserted in the sample. The catalyst was first activated *in situ* under $H_2$ (100 mL $min^{-1}$) at 350 °C and cooled down to 90 °C. The gas flow was then switched to He (100 mL $min^{-1}$) for 10 min. The adsorption/desorption of $N_2O$ at T = 90 °C on the copper containing catalyst was studied according to the following switches: He (100 mL $min^{-1}$) → 2% $N_2O$/2% Ar/He (100 mL $min^{-1}$) providing the total amount of adsorbed $N_2O$ species and $N_2$ production. The flow (100 mL $min^{-1}$) was switched to He, then 2% $N_2O$/2% Ar/He, then back to He in order to verify the absence of weakly adsorbed species and attest of the saturation of the sites. Previous to analyses, gas mixtures of known compositions were used for the calibration of the MS and the ascertainment of the linearity of the response of the gases used in the present study: $N_2O$, $N_2$ and Ar. $N_2O$ chemisorbed ($n_{N2Ochem}$, mol) correspond to the amount of $N_2O$ consumed which is calculated based on the molar fraction of $N_2O$ at the inlet and outlet of the reactor. The molar flow rate of Ar serves as reference.

The concentration of accessible Cu sites ($Cu_s$, expressed in $mol_{Cu}$ $g^{-1}$) were estimated based on $N_2O$ chemisorbed, with a stoichiometry of $Cu_s$:O estimated to be 2:1 using the following equation:[51]

$$Cu_S = \frac{2 \times n_{N2Ochem}}{m_{catalyst}} \text{ [eq. (1)]}$$

The specific Cu surface area ($Cu_{exp}$, expressed in $m^2_{Cu}$ $g^{-1}_{Cu}$) of the materials were then determined based on $N_2O$ chemisorbed, the mass of Cu in the sample ($m_{Cu}$, g), $N_A$ the Avogadro's number, and the copper surface density ($\rho_s$ = 1.46 × $10^{19}$ atoms $m^2$) according to:[74]

$$Cu_{exp} = \frac{2 \times n_{N2Ochem} \times N_A}{m_{Cu} \times \rho_S} \text{ [eq. (2)]}$$

The mean particles sizes ($d_{Cu,\ N2O}$, expressed in nm) were calculated based on eq. (3) assuming spherical particles:

$$d_{Cu,N2O} = \frac{6000}{Cu_{exp} \times \rho_{Cu}} \text{ [eq. (3)]}$$

with $\rho_{Cu}$ the Cu metal density (8.94 g $cm^{-3}$) and $Cu_{exp}$ expressed in $m^2_{Cu}$ $g^{-1}_{Cu}$.

Analysis of the acidic properties of $Cu/ZnAl_xO_y$ samples was performed by adsorption of pyridine follow by infrared spectroscopy. Before analysis, samples were pressed at ~1 ton $cm^{-2}$ into thin wafers of 5 to 8 mg $cm^{-2}$ and placed inside the IR cell. Before pyridine adsorption/desorption experiments, the wafers were treated under $H_2$(5%)/Ar flow (30 mL $min^{-1}$) at 350°C (ramp: 5 °C $min^{-1}$) for 1 h and then outgassed under secondary vacuum at 350°C for 1 h. Wafers were then contacted at 150°C with gaseous pyridine (approximately 133 Pa) via a separate cell containing liquid pyridine. The spectra were then recorded following desorption from 150 to 300 °C with a Bruker Vector 22 spectrometer (resolution 4 $cm^{-1}$, 64 scans). The reported spectra were obtained after subtraction of the spectrum recorded before pyridine adsorption and normalization at 10 mg $cm^{-2}$. The amount of Lewis acidic centers titrated by pyridine was obtained using a molar absorption coefficient value of $\varepsilon$ = 1.71 cm $\mu mol^{-1}$ for the $\nu_{19b}$ vibration of coordinated pyridine (Py-L) at ~1450 $cm^{-1}$.[75]

**Catalytic tests**

The glycerol hydrogenolysis was performed using a 300 mL reactor autoclave. Typically, 100 mL of glycerol aqueous solution (2.14 wt%) and 0.5 g of catalyst were loaded into the reactor. After sealing, the autoclave was purged three times with Ar. Then the heating was turned on to reach 200 °C, and the stirring was started. When the temperature was stable, 30 bar of hydrogen was added into the reactor (total pressure of the reactor = 46 bar).

The operating conditions were chosen to ensure negligible mass transport limitation. The stirring was set at 1000 rpm in order to avoid interphase diffusion limitation. Isothermal conditions (± 1 °C) were ensured by working in diluted solution. The $H_2$ content in a aqueous solution under our reaction conditions is around 0.067 mol $L^{-1}$ based on Henry's law constant[76], hence the initial molar fraction $X_{H2}/_{glycerol}$ is ca. 30%. $H_2$ was periodically added during the reaction in order to maintain the pressure constant and an excess of $H_2$. Liquid samples were collected periodically during the reaction (up to 24 h) and analyzed by gas chromatography (Shimadzu GC-2010 with a AOC-20s Auto Sampler, column ZB-FFAP 30 m × 0.32 mm × 0.25 µm, $N_2$ as carrier gas, FID detector). The concentrations of the products were determined after calibration. At the end of the reaction, the autoclave was cooled down, the pressure was released, and the suspension was collected and filtered.

The conversion of glycerol as well as the selectivity and yield were calculated based on the concentration of the substrate at time 0 and t, in liquid products. The carbon selectivity $S_t^i$ to a desired product was based on the concentration of product and substrate at time t, and the number of carbon atoms.[46] Repeated reactions delivered conversion reproducible within ± 3%. The selectivity is given with an absolute accuracy of ± 3%. The initial reaction rate ($V_0$, ± 0.3 $mmol_{gly}$ $g^{-1}_{Cu}$ $h^{-1}$) was calculated based on the slope of the linear part of the curve (conversion = f(t)) at low conversion (< 40%).

**Acknowledgments**

L.O. acknowledges the Lebanese association Daw for the financial support. The authors thank in particular Thibaut Cornier and the members of the IRCELYON scientific platforms

IRTECH for their assistance in the characterization of catalysts. Thanks to Christelle Fabrer-Boulé and the Centre Technologique des Microstructures (CTμ) for the SEM analyses.

**Conflict of Interest**

The authors declare no conflict of interest.

**References**

[1] *Glycerol: A Versatile Renewable Feedstock for the Chemical Industry*, (Ed.: C. J. A. Mota, B. P. Pinto, A.L. de Lima), Springer, New York, **2017**, pp. 93-103.

[2] M. Checa, S. Nogales-Delgado, V. Montes, J. M. Encinar, *Catalysts* **2020**, *10*, 1279.

[3] S. Wang, K. Yin, Y. Zhang, H. Liu, *ACS Catal.* **2013**, *3*, 2112.

[4] Y. Kusunoki, T. Miyazawa, K. Kunimori, K. Tomishige, *Catal. Commun.* **2005**, *6*, 645.

[5] Z. Wu, Y. Mao, X. Wang, M. Zhang, *Green Chem.* **2011**, *13*, 1311.

[6] A. L. Chun Minh, S. P. Samudrala, S. Bhattacharya, *Sustainnable Energy Fuels* **2022**, *6*, 596.

[7] A. M. Ruppert, K. Weinberg, R. Palkovits, *Angew. Chem., Int. Ed.* **2012**, *51*, 2564.

[8] X. Liu, B. Yin, W. Zhang, X. Yu, Y. Du, S. Zhao, G. Zhang, M. Liu, H. Yan, M. Abbotsi- Dogbey, S. T. Al- Absi, S. Yeredil, C. Yang, J. Shen, W. Yan, X. Jin, *Chem. Rec.* **2021**, *21*, 1792.

[9] Q. Gao, B. Xu, Q. Tong, Y. Fan, *Biosci., Biotechnol., Biochem.* **2016**, *80*, 215.

[10] S. Wang, H. Liu, *Catal. Lett.* **2007**, *117*, 62.

[11] M. Balaraju, V. Rekha, P. S. Sai Prasad, R. B. N. Prasad, N. Lingaiah, *Catal. Lett.* **2008**, *126*, 119.

[12] Y. Du, C. Wang, H. Jiang, C. Chen, R. Chen, *J. Ind. Eng. Chem.* **2016**, *35*, 262.

[13] C.-J. Yue, Q.-Y. Zhang, L.-P. Gu, Y. Su, S.-P. Zhu, *Asia-Pac. J. Chem. Eng.* **2014**, *9*, 581.

[14] A. Żelazny, K. Samson, R. Grabowski, M. Śliwa, M. Ruggiero-Mikołajczyk, A. Kornas, *React. Kinet., Mech. Catal.* **2017**, *121*, 329.

[15] I. C. Freitas, R. L. Manfro, M. M. V. M. Souza, *Appl. Catal., B* **2018**, *220*, 31.

[16] T. Auttanat, S. Jongpatiwut, T. Rirksomboon, *Int. J. Chem. Mol. Eng.* **2012**, *6*, 297.

[17] S. Zhu, X. Gao, Y. Zhu, Y. Li, *Green Chem* **2016**, *18*, 782.

[18] A. Bienholz, H. Hofmann, P. Claus, *Appl. Catal., A* **2011**, *391*, 153.

[19] E. S. Vasiliadou, A. A. Lemonidou, *Appl. Catal., A* **2011**, *396*, 177.

[20] Z. Huang, F. Cui, J. Xue, J. Zuo, J. Chen, C. Xia, *Catal. Today* **2012**, *183*, 42.

[21] S. Zhu, X. Gao, Y. Zhu, W. Fan, J. Wang, Y. Li, *Catal. Sci. Technol.* **2015**, *5*, 1169.

[22] V. Rekha, N. Raju, C. Sumana, S. Paul Douglas, N. Lingaiah, *Catal. Lett.* **2016**, *146*, 1487.

[23] T. Gabrysch, B. Peng, S. Bunea, G. Dyker, M. Muhler, *ChemCatChem* **2018**, *10*, 1344.

[24] G. Luciani, G. Ruoppolo, G. Landi, V. Gargiulo, M. Alfè, A. Di Benedetto, *Catalysts* **2022**, *12*, 72.

[25] A. A. A, S. Mondal, S. M. Pudi, N. N. Pandhare, P. Biswas, *Energy Fuels* **2017**, *31*, 8521.

[26] B. Mallesham, P. Sudarsanam, B. V. S. Reddy, B. M. Reddy, *Appl. Catal., B* **2016**, *181*, 47.

[27] Z. Yuan, J. Wang, L. Wang, W. Xie, P. Chen, Z. Hou, X. Zheng, *Bioresour. Technol.* **2010**, *101*, 7088.

[28] M. Balaraju, K. Jagadeeswaraiah, P. S. S. Prasad, N. Lingaiah, *Catal. Sci. Technol.* **2012**, *2*, 1967.

[29] J. Chaminand, L. aurent Djakovitch, P. Gallezot, P. Marion, C. Pinel, C. Rosier, *Green Chem.* **2004**, *6*, 359.

[30] A. Bienholz, F. Schwab, P. Claus, *Green Chem* **2010**, *12*, 290.

[31] D. Durán-Martín, M. L. Granados, J. L. G. Fierro, C. Pinel, R. Mariscal, *Top. Catal.* **2017**, *60*, 1062.

[32] C. Wang, H. Jiang, C. Chen, R. Chen, W. Xing, *Chem. Eng. J.* **2015**, *264*, 344.

[33] M. Hou, H. Jiang, Y. Liu, R. Chen, *React. Kinet., Mech. Catal.* **2017**, *122*, 1129.

[34] L. C. Meher, R. Gopinath, S. N. Naik, A. K. Dalai, *Ind. Eng. Chem. Res.* **2009**, *48*, 1840.

[35] S. Panyad, S. Jongpatiwut, T. Sreethawong, T. Rirksomboon, S. Osuwan, *Catal. Today* **2011**, *174*, 59.

[36] D. W. Kim, S. H. Ha, M. J. Moon, K. T. Lim, Y. B. Ryu, S. D. Lee, M. S. Lee, S.-S. Hong, *J. Nanosci. Nanotechnol.* **2015**, *15*, 656.

[37] D. Jean, B. Nohair, J.-Y. Bergeron, S. Kaliaguine, *Ind. Eng. Chem. Res.* **2014**, *53*, 18740.

[38] S. Wang, H. Liu, *Chin. J. Catal.* **2014**, *35*, 631.

[39] Z. Zhou, X. Li, T. Zeng, W. Hong, Z. Cheng, W. Yuan, *Chin. J. Chem. Eng.* **2010**, *18*, 384.

[40] R. B. Mane, S. E. Kondawar, P. S. Niphadkar, P. N. Joshi, K. R. Patil, C. V. Rode, *Catal. Today* **2012**, *198*, 321.

[41] H. Tan, M. N. Hedhill, Y. Wang, J. Zhang, K. Li, S. Sioud, Z. A. Al-Talla, M. H. Amad, T. Zhan, O. E. Tall, Y. Han, *Catal. Sci. Technol.* **2013**, *3*, 3360.

[42] V.-L. Yfanti, E. S. Vasiliadou, A. A. Lemonidou, *Catal. Sci. Technol.* **2016**, *6*, 5415.

[43] R. D. Gonzalez, T. Lopez, R. Gomez, *Catal. Today* **1997**, *35*, 293.

[44] W. Zou, R. D. Gonzalez, *Appl. Catal., A* **1995**, *126*, 351.

[45] W. Zou, R. D. Gonzalez, *J. Catal.* **1995**, *152*, 291.

[46] L. Omar, N. Perret, S. Daniele, *Catalysts* **2021**, *11*, 516.

[47] S. Derrouiche, H. Lauron-Pernot, C. Louis, *Chem. Mater.* **2012**, *24*, 2282.

[48] M. N. Barroso, M. F. Gomez, J. A. Gamboa, L. A. Arrúa, M. C. Abello, *J. Phys. Chem. Solids* **2006**, *67*, 1583.

[49] V.-L. Yfanti, A. A. Lemonidou, *Catal. Today* **2020**, *355*, 727.

[50] Y. Liu, N. Pasupulety, K. Gunda, G. L. Rempel, F. T. T. Ng, *Top. Catal.* **2014**, *57*, 1454.

[51] O. Hinrichsen, T. Genger, M. Muhler, *Chem. Eng. Technol.* **2000**, *23*, 956.

[52] C. Morterra, G. Magnacca, *Catal. Today* **1996**, *27*, 497.

[53] G. Busca, *Adv. Catal.* **2014**, *57*, 319.

[54] P. F. Rossi, G. Busca, V. Lorenzelli, M. Waqif, O. Saur, J. C. Lavalley, *Langmuir* **1991**, *7*, 2677.

[55] C. Morterra, G. Cerrato, *Catal. Lett.* **1991**, *10*, 357.

[56] J.-C. Lavalley, J. Caillod, *J. Chim. Phys.* **1980**, *77*, 373.

[57] H. Stolz, H. Knözinger, *Kolloid Z. Z. Polym.* **1971**, *243*, 71.

[58] A. B. M. Saad, V. A. Ivanov, J. C. Lavalley, *Appl. Catal., A* **1993**, *94*, 71.

[59] C. Morterra, S. Coluccia, E. Garrone, G. Ghiotti, *J. Chem. Soc., Faraday Trans. 1* **1979**, *75*, 289.

[60] W. Zhang, Y. Wang, Y. Shen, M. Xie, X. Guo, *Microporous Mesoporous Mater.* **2016**, *226*, 278.

[61] M. N. Gatti, N. N. Nichio, F. Pompeo, *Reactions* **2022**, *3*, 451.

[62] Z. Wu, Y. Mao, M. Song, X. Yin, M. Zhang, *Catal. Commun.* **2013**, *32*, 52.

[63] L. Huang, Y.-L. Zhu, H.-Y. Zheng, Y.-W. Li, Z.-Y. Zeng, *J. Chem. Technol. Biotechnol.* **2008**, *83*, 1670.

[64] S. Guadix-Montero, A. Santos-Hernandez, A. Folli, M. Sankar, *Philos. Trans. R. Soc., A* **2020**, *378*, 20200055.

[65] V. Montes, M. Checa, A. Marinas, M. Boutonnet, J. M. Marinas, F. J. Urbano, S. Järas, C. Pinel, *Catal. Today* **2014**, *223*, 129.

[66] D. D. Falcone, J. H. Hack, A. Yu. Klyushin, A. Knop-Gericke, R. Schlögl, R. J. Davis, *ACS Catal.* **2015**, *5*, 5679.

[67] H. Du, S. Chen, H. Wang, J. Lu, *Chin. J. Catal.* **2017**, *38*, 1237.

[68] R. M. West, D. J. Braden, J. A. Dumesic, *J. Catal.* **2009**, *262*, 134.

[69] V. Bolis, C. Morterra, M. Volante, L. Orio, B. Fubini, *Langmuir* **1990**, *6*, 695.

[70] R. Wischert, P. Laurent, C. Copéret, F. Delbecq, P. Sautet, *J. Am. Chem. Soc.* **2012**, *134*, 14430.

[71] R. Wischert, C. Copéret, F. Delbecq, P. Sautet, *Angew. Chem.* **2011**, *123*, 3260.

[72] E. van Ryneveld, A. S. Mahomed, P. S. van Heerden, M. J. Green, C. Holzapfel, H. B. Friedrich, *Catal. Sci. Technol.* **2014**, *4*, 832.

[73] Y. Wang, J. Zhou, X. Guo, *RSC Adv.* **2015**, *5*, 74611.

[74] G. Bergeret, P. Gallezot, *Particle Size Dispersion Measurements in Handbook of Heterogeneous Catalysis*, Vol. 2 (Eds.: G. Ertl, H. Knözinger, J. Weitkamp), Wiley-VCH, Weinheim, **1997**, pp.439-442.

[75] V. Zholobenko, C. Freitas, M. Jendrlin, P. Bazin, A. Travert, F. Thibault-Starzyk, *J. Catal.* **2020**, *385*, 52.

[76] T.-K.-H. Trinh, J.-C. de Hemptinne, R. Lugo, N. Ferrando, J.-P. Passarello, *J. Chem. Eng. Data* **2016**, *61*, 19–34.

## Table of contents

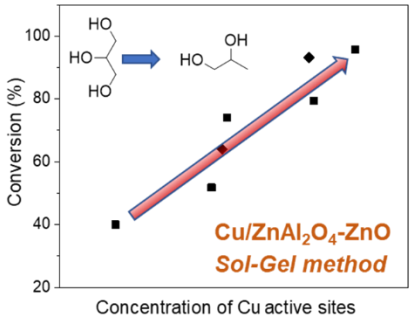


Novel Sol-gel method for Cu / Zinc Aluminate as catalyst for glycerol hydrogenolysis. The presence of polyacrylic acid and aluminium during the synthesis improved the catalytic properties. Conversions up to 96% with selectivity towards 1,2-propanediol of 83% were obtained.